AD_____

Award Number: W81XWH-06-1-0210

TITLE: Noninvasive Localization of Prostate Cancer via Diffusion Sensitive MRI

PRINCIPAL INVESTIGATOR: Junqian Xu

CONTRACTING ORGANIZATION: Washington University
Saint Louis, MO 63110

REPORT DATE: March 2007

TYPE OF REPORT: Annual Summary

PREPARED FOR: U.S. Army Medical Research and Materiel Command
Fort Detrick, Maryland 21702-5012

REPORT DOCUMENTATION PAGE

Form Approved
OMB No. 0704-0188

1. REPORT DATE	2. REPORT TYPE	3. DATES COVERED
01-03-2007	Annual Summary	15 Feb 2006 – 14 Feb 2007

4. TITLE AND SUBTITLE

Noninvasive Localization of Prostate Cancer via Diffusion Sensitive MRI

5a. CONTRACT NUMBER

5b. GRANT NUMBER
W81XWH-06-1-0210

5c. PROGRAM ELEMENT NUMBER

6. AUTHOR(S)

Junqian Xu

Email: jxu@wustl.edu

5d. PROJECT NUMBER

5e. TASK NUMBER

5f. WORK UNIT NUMBER

7. PERFORMING ORGANIZATION NAME(S) AND ADDRESS(ES)

Washington University
Saint Louis, MO 63110

8. PERFORMING ORGANIZATION REPORT NUMBER

9. SPONSORING / MONITORING AGENCY NAME(S) AND ADDRESS(ES)
U.S. Army Medical Research and Materiel Command
Fort Detrick, Maryland 21702-5012

10. SPONSOR/MONITOR'S ACRONYM(S)

11. SPONSOR/MONITOR'S REPORT NUMBER(S)

12. DISTRIBUTION / AVAILABILITY STATEMENT
Approved for Public Release; Distribution Unlimited

13. SUPPLEMENTARY NOTES
Original contains colored plates: ALL DTIC reproductions will be in black and white.

14. ABSTRACT Diffusion tensor magnetic resonance imaging (DTI) measurements of prostate cancer (PCa) were performed in vivo, in patients undergoing radical prostatectomy, and ex vivo, in the same patients' prostatectomy specimens. For the first time, the imaging data were co-registered to histological sections of the prostatectomy specimens, thereby enabling unambiguous characterization of diffusion parameters in cancerous and benign tissues. Through image co-registration and histological analysis, we have shown that increased cellularity, and thence decreased luminal spaces, in peripheral zone PCa leads to about 40 % and 50 % apparent diffusion coefficient (ADC) decrease compared to benign peripheral zone tissues in vivo and ex vivo, respectively. In contrast, no significant diffusion anisotropy differences between the cancerous and non-cancerous peripheral zone tissues were observed. The bundled fibromuscular tissues in prostate, such as stromal tissues in benign prostatic hyperplasia (BPH), exhibited high diffusion anisotropy facilitating the differentiation of PCa from BPH in central gland. A tissue classification method, combining DTI and T2w images, was proposed to provide more specific PCa detection. An ADC threshold for PCa was also established to provide unsupervised PCa localization. The PCa identified using this method correlate well with histologically identified PCa foci.

15. SUBJECT TERMS
magnetic resonance imaging (MRI), diffusion tensor imaging (DTI), apparent diffusion coefficient (ADC), relative anisotropy (RA), prostate carcinoma (PCa), and benign prostatic hyperplasia (BPH)

16. SECURITY CLASSIFICATION OF:			17. LIMITATION OF ABSTRACT	18. NUMBER OF PAGES	19a. NAME OF RESPONSIBLE PERSON
a. REPORT	b. ABSTRACT	c. THIS PAGE			USAMRMC
U	U	U	UU	40	19b. TELEPHONE NUMBER *(include area code)*

Table of Contents

Introduction

Current curative strategies for prostate cancer (PCa) focus on the detection and treatment of early-stage tumors (*1*). However, the standard method of diagnosis, transrectal ultrasound guided needle biopsy, misses 20 – 30 % of clinically significant tumors (*2*). Repeated negative biopsies do not guarantee that the patient is cancer free. Although magnetic resonance imaging (MRI) provides excellent soft-tissue contrast of the prostate, the standard T2-weighted (T2w) MRI is not sensitive or specific enough for accurate PCa localization (*1, 3*). In an earlier study from this laboratory, the lower water apparent diffusion coefficient (ADC) of PCa compared to benign prostate tissues markedly improved contrast of PCa *vs.* non-cancerous prostate tissue in a transgenic mouse model *in vivo (4)*. In this pre-doctoral project awarded by Department of Defense, we proposed to investigate the ADC contrast by diffusion tensor MRI (DTI) in gland confined human PCa for improved detection and localization. The ADC and relative diffusion anisotropy of water, parameters derived from DTI (*5*), reflect tissue microstructure at the micron scale and hence are sensitive to pathologic changes. This proposal is based on the **hypothesis** that the water ADC differential between PCa and benign prostate tissues will provide the desired contrast *in vivo* for noninvasive PCa detection in patients *via* diffusion sensitive MRI. The **objective** of this work is to demonstrate that tumor foci within the prostate may be accurately identified using water ADC. Diffusion sensitive MRI, as a noninvasive method, shows the potential to accurately localize tumor foci within the prostate. Our current results have an immediate **impact** in (i) enabling MRI guided targeted needle biopsy, thus, reducing the incidence of false negative results and the need for saturation biopsy, (ii) supporting focal ablation techniques, thus, reducing the need for whole prostate resection (*6*), and (iii) providing a tool for watchful waiting and post-therapy monitoring.

Body

Aim 1: To confirm the existance and quantify the extent *in vivo* of a large (~2 fold) water ADC differential between PCa and benign human prostate tissues. This differential is expected from (i) a previous published transgenic mouse study (*4*), (ii) a recent study with resected human prostates (*7*), and (iii) preliminary human data acquired *in vivo (8)*.

The major progress in this funding period is in data analysis. We have achieved **Aim 1** by analyzing the *in vivo*, *ex vivo* DTI, and histology data acquired prior to this funding period. Although we have proposed to collect data from 12 patients in *Task 1* (PCa localization with radical prostatectomy patients expressing significant pathology.) in the statement of work (SOW), no patient data were acquired during this funding period. The reasons for this delay in patient recruitments are the following. First, we have collected enough preliminary data during the DOD administrative delay (i.e., application granted on Jul. 14 2005 - funding issued on Feb. 15 2006) through the departmental support for analysis and to achieve a statistical significance. Second, modifications to the existing study protocol were required by the DOD. This required resubmission to the Washington

University IRB, which is taking much longer than expected. Because of these administrative procedural delays, the patient enrollment was suspended.

Twenty four patients undergoing radical prostatectomy (mean age 62 years; range 46 - 76 years) who had not received any preoperative treatment such as androgen ablation or radiation therapy were recruited in this study (note: usable data obtained from patients recruited for a different project with appropriate IRB approval). The prostates of 14 patients, of which 12 had significant tumor burden (> 5%), were examined using DTI both *in vivo*, prior to surgery, and *ex vivo*, after resection (Appendix I.). The prostates of the other 10 patients, of which 4 had significant tumor burden (> 5%), were examined only *ex vivo*, after resection. The 16 patients with post-surgery histology determined (Appendix I.) significant tumor burden (mean volume 20%, range 5% - 46%) had a median post-resection Gleason score of 3 + 4 = 7 (range 3 + 3 = 6 to 4 + 5 = 9).

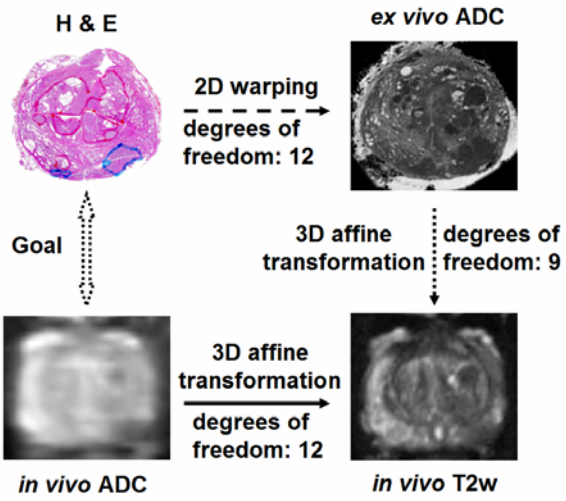

Figure 1. Overview of histology and MR co-registration scheme.

We have implemented the proposed co-registration strategy (Appendix I.) to fuse *in vivo*, *ex vivo* DTI, and optical images of histology slide (Fig. 1). A match of alignment (orientation and position) between histology slides and *in vivo* ADC slices in the standard *in vivo* T2w image space was achieved for purposes of translating the histology identified PCa regions onto the *in vivo* MR images (Fig. 2).

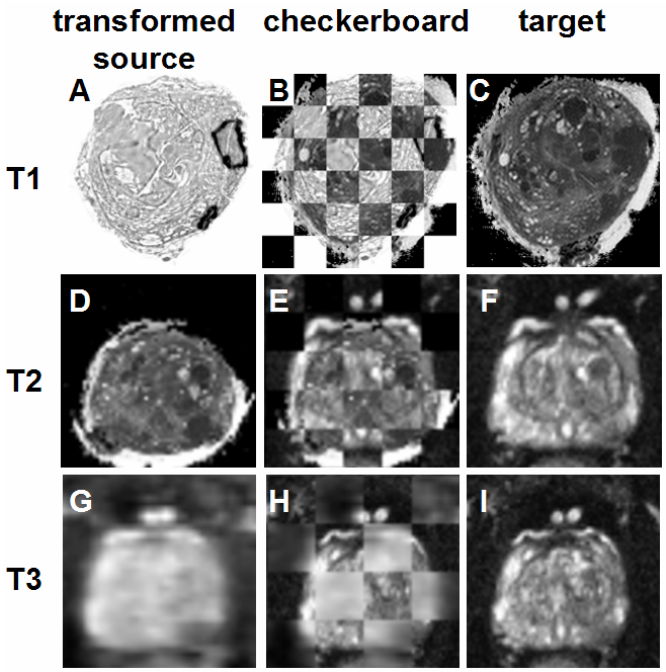

Figure 2. Registration results at three transformation stages (rows, T1 - T3). The transformed source images (left column) were overlaid onto the target images (right column) with the alignment results highlighted as checkerboards (center column) for visualizing the goodness of the transformation. The transformation pairs are A) TPS warped H & E and C) *ex vivo* ADC; D) transformed *ex vivo* ADC and F) *in vivo* T2W; and G) transformed *in vivo* ADC and I) *in vivo* T2w.

After image registration, cancerous and normal tissues in the peripheral zone (PZ) were translated from the histology slides onto the *in vivo* and *ex vivo* ADC maps to determine the ADC values in each tissue category (Fig. 3A and D). The ADC values in PCa are consistently much lower than that in normal tissues in patients *in vivo*, and *ex vivo* prostatectomy specimens (Appendix I.). This is consistent with *in vivo* mouse model of PCa (Fig. 4). Similarly relative diffusion anisotropy (sRA) can be determined for all tissue regions. Although no significant diffusion anisotropy differences between the cancerous and non-cancerous PZ tissues were observed (Fig. 3), the bundled fibromuscular tissues in prostate, such as stromal tissues in benign prostatic hyperplasia (BPH), exhibited high diffusion anisotropy facilitating the differentiation of PCa from BPH in central gland (Fig. 3C and F red arrows, and Appendix I. Fig. 4). A tissue classification method, combining DTI and T2w images, was proposed to provide a more specific PCa detection (Appendix I. Table 1).

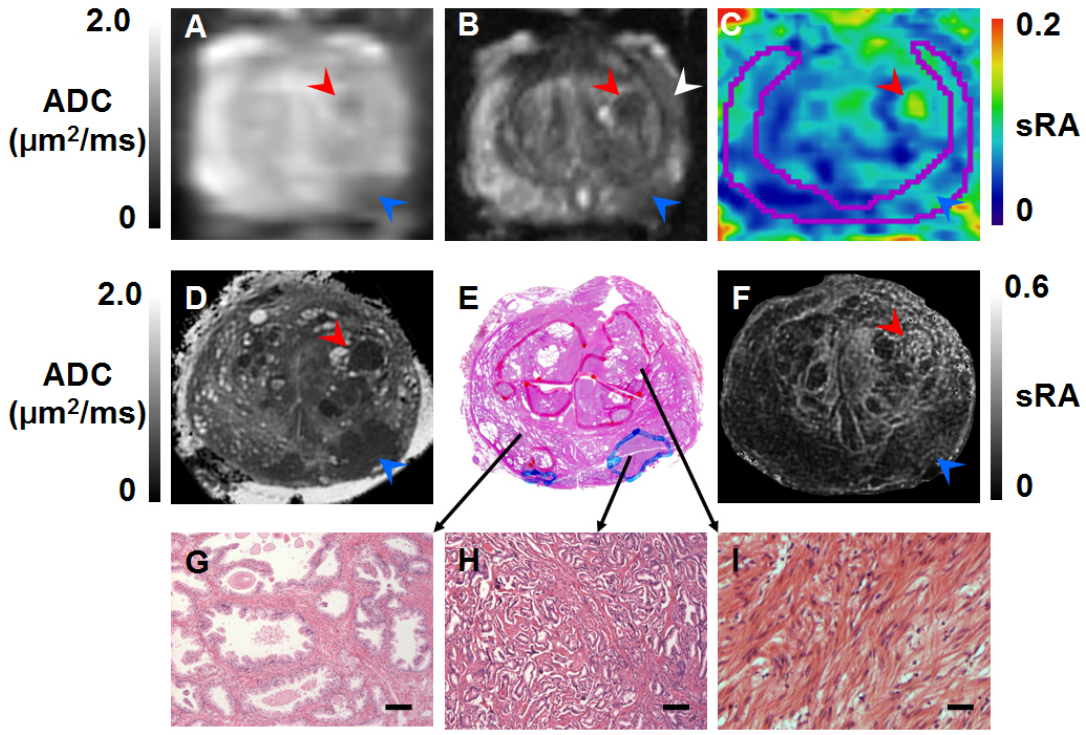

Figure 3. Co-registered images illustrate the tissue microstructure underpinning the MR diffusion characteristics. A) *in vivo* ADC, B) *in vivo* T2w, C) *in vivo* color coded sRA, D) *ex vivo* ADC, E) H & E slide, and F) *ex vivo* sRA. The cancerous and BPH regions in the H & E slide were marked in blue and red, respectively, by a urologic pathologist. Blue and red arrows indicate regions of PCa and stromal BPH, respectively, as diagnosed by histology. The white arrow in panel B indicates a T2 hypointense region that could be mistaken for PCa without the additional co-registered diffusion data. The peripheral zone were delineated in panel B and mapped onto panel C in magenta. High resolution H & E examinations reveal the micro-structures of different types of tissues in G) benign peripheral zone, H) PCa, and I) stromal BPH (10× magnification, scale bar = 100 μm).

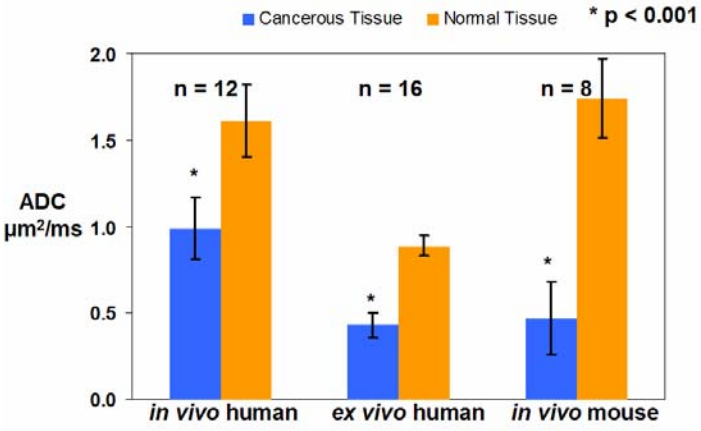

Figure 4. Lower ADC values were observed in patients *in vivo*, *ex vivo* prostatectomy specimens, and an *in vivo* mouse model of PCa. All results were determined by histopathology identified tissue categories. Error bars represent standard deviation. Statistical significance was accepted for $p < 0.001$.

An ADC threshold for PCa was established based on the results in Fig. 4 to provide unsupervised PCa localization. The PCa identified using this method correlate well with histologically identified PCa foci (Appendix I. Fig. 5 and 6).

In summary, through histology analysis and image co-registration, we have validated the existance and quantified the extent of a large (~ 2 fold) water ADC differential between PCa and benign peripheral zone human prostate tissues *in vivo*. The diffusion anisotropy, derived from DTI, was also quantified in prostate through the analysis. Combining DTI and T2w contrasts has the potential to provide specific PCa detection and accurate PCa localization.

<u>Technical Development:</u> *In vivo* diffusion MRI optimization with endo-rectal coil.

In vivo diffusion MRI in human prostate is technically challenging for its small size, its central location inside the body, the surrounding fat, and respiratory motion. Image distortion and blurring commonly plagues diffusion weighted images (DWI) of the prostate and consequently the calculated ADC map. We have used a phased-array body coil for MR signal reception. Although image distortion is minimum by using the body coil, low SNR limits achievable image resolution with a prolonged scan time approaching 30 min. Such a lengthy acquisition leads to image blurring because of patient motion (Fig. 5C). In close consultation with Radiology Professor Vamsidhar Narra, M.D., (one of the co-investigators of this pre-doctoral fellowship), the trainee has explored the possible use of an

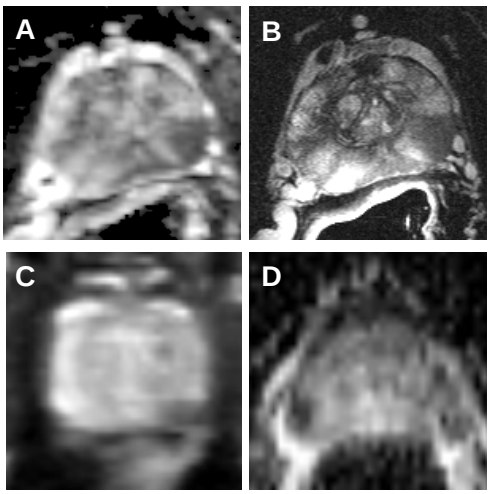

Figure 5. Diffusion MR image quality comparison. (A) ADC by optimized endo-rectal coil diffusion protocol, (B) corresponding T2w image, (C) ADC by optimized body coil diffusion protocol, and (D) ADC by non-optimized endo-rectal coil diffusion protocol.

endo-rectal coil for diffusion sensitive MRI in the upcoming study. Use of the endo-rectal coil holds promise of substantially higher image signal-to-noise ratio (SNR) than available with the body-phased array coil initially proposed. Consequently, the diffusion scan time decreased to a clinically more acceptable 10-min acquisition. However, the endo-rectal coil usually exaggerates susceptibility induced artifacts. These significantly distort the diffusion image when using a non-optimized pulse sequence and imaging protocol (Fig. 5D). Although our ability to recruit patients was limited due to IRB approval delay, we have taken time to optimize the MRI diffusion pulse sequence/protocol on a phantom. As a result, in one of the clinical cases, the intraglandular features and contrast in the ADC map (Fig 5A) reflect those seen in the high resolution T2w image (Fig. 5B). Image distortion was minimized. Achieving such high-quality diffusion images will improve the PCa detection limit using the ADC contrast, which is to be investigated in Aim 2.

The trainee has continued to improve the applicable MR pulse sequences, leading to better *in vivo* image quality. By optimizing the spin echo echo-planar imaging (SE-EPI) diffusion sequence with the inner volume imaging (IVI) technique (*9*, *10*), we have significantly improved the quality of diffusion weighted images from phantom (test) samples (Fig. 6). Currently, due to technical limitations on the Siemens scanner, both body coils and endo-rectal coil have to be enabled to collect diffusion data. The recently developed IVI diffusion sequence by the trainee (*11*) with zoom-in ability eliminates the need for the body coils during reception and, hence, will result in less noise contamination. In a phantom test, the endo-rectal coil receive-only DWI (Fig. 4B) shows significantly higher signal-to-noise ratio (SNR) and a less structured noise profile than body and endo-rectal coil receive-combined DWI (Fig. 4A). We will implement this endo-rectal coil receive-only data acquisition using this optimized IVI diffusion sequence in the upcoming study. This will eliminate whole body radio-frequency (RF) noise emanating from the body coils.

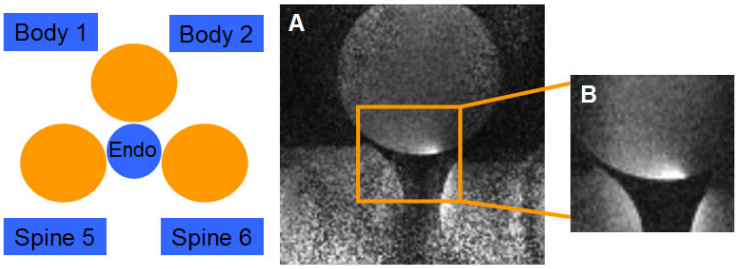

Figure 6. Comparison of body-endorectal coils receive-combined and endorectal coil receive-only data acquisition in phantom tests. Left cartoon: RF coil elements (blue) configuration and phantom (orange) placement corresponding to human prostate MRI. (A) DWI with all five coil elements combined, and (B) DWI with endo-rectal coil only.

In summary, we have improved our *in vivo* diffusion image quality by using the endo-rectal coil and an optimized diffusion sequence/protocol. The improved SNR, reduced image distortion and blurring, as well as the reduction in scan time, will have significant impact on quantifying the PCa detection limit as proposed in Aim 2.

Aim 2: To quantify the accuracy and limitation of *in vivo* ADC-based MRI tumor detection and localization. *In vivo* human MRI data will be compared with very high signal-to-noise/resolution MRI data acquired on the same prostate following resection and with histologic analysis by a clinical pathologist.

We are now waiting for local IRB approval and, subsequently, the secondary DOD approval to start patient enrollment. We expect this process to be completed shortly and to embark on the second aim of this proposed study.

Key Research Accomplishments

1. For the first time, the imaging data were co-registered to histological sections of the prostatectomy specimens, thereby enabling unambiguous characterization of diffusion parameters in cancerous and benign tissues. Through image co-registration and histological analysis, we have shown that increased cellularity, and hence decreased luminal spaces, in peripheral zone PCa leads to ~ 40 % and 50 % ADC decrease compared to benign peripheral zone tissues *in vivo* and *ex vivo*, respectively.

2. No significant diffusion anisotropy differences between the cancerous and non-cancerous peripheral zone tissues were observed.

3. The bundled fibromuscular tissues in prostate, such as stromal tissues in benign prostatic hyperplasia (BPH), exhibited high diffusion anisotropy facilitating the differentiation of PCa from BPH in central gland.

4. An ADC threshold for PCa was established to provide unsupervised PCa localization. The PCa identified using this method correlate well with histologically identified PCa foci.

5. A tissue classification method, combining DTI and T2w images, was proposed to provide more specific PCa detection.

6. The *in vivo* diffusion image quality was significantly improved by using an endo-rectal coil and an optimized diffusion sequence/protocol developed by the trainee. As a result, the improved SNR, reduced image distortion and blurring, as well as the reduction in scan time will have significant impact on the upcoming study.

Reportable Outcomes

1. Manuscript "Magnetic Resonance Diffusion Characteristics of Histologically Defined Prostate Cancer in Human" **J. Xu**, P. A. Humphrey, A. S. Kibel, A. Z. Snyder, V. R. Narra, J. J. H. Ackerman, and S. K. Song *Cancer Research*, in preparation

2. Abstract and Electronic-Poster Presentation "ADC Decrease in Histology Identified Prostate Cancer" **J. Xu**, P. A. Humphrey, A. S. Kibel, A. Z. Snyder, V. R. Narra, and S. K. Song. *Proc. Intl. Soc. Magn. Reson. Med.* 15, Accepted, 2007

3. Abstract and Oral Presentation "Exclusion of False Positive Identification of Prostate Cancer Using Diffusion Anisotropy" **J. Xu**, P. A. Humphrey, A. S. Kibel, V. R. Narra, and S. K. Song. *Proc. Intl. Soc. Magn. Reson. Med.* **14**, 174, 2006

Conclusion

We have made significant progress during this funding period by analyzing the preliminary data acquired prior to this funding period. Our proposed first aim has been achieved with statistical significance. Our *in vivo* diffusion MRI data acquisition sequence/protocol was significantly improved during this funding period, as well. This enables us to better address our proposed second aim. The results presented in this progress report positively impact the use of diffusion sensitive MRI to accurately localize PCa *in vivo*.

References

1. Kantoff, P. W., Rarroll, P. R., and D'Amico, A. V. (eds.) Prostate Cancer: Principles & Practice, 1st edition, p. 278-280. Philadelphia: Lippincontt Williams & Wilkins, 2002.
2. Keetch, D. W., Catalona, W. J., and Smith, D. S. Serial prostatic biopsies in men with persistently elevated serum prostate specific antigen values. J Urol, *151:* 1571-1574, 1994.
3. Coakley, F. V., Qayyum, A., and Kurhanewicz, J. Magnetic resonance imaging and spectroscopic imaging of prostate cancer. J Urol, *170:* S69-75; discussion S75-66, 2003.
4. Song, S. K., Qu, Z., Garabedian, E. M., Gordon, J. I., Milbrandt, J., and Ackerman, J. J. Improved magnetic resonance imaging detection of prostate cancer in a transgenic mouse model. Cancer Res, *62:* 1555-1558, 2002.
5. Basser, P. J. and Pierpaoli, C. Microstructural and physiological features of tissues elucidated by quantitative-diffusion-tensor MRI. J Magn Reson B, *111:* 209-219, 1996.
6. Katz, A. E. and Rewcastle, J. C. The current and potential role of cryoablation as a primary therapy for localized prostate cancer. Curr Oncol Rep, *5:* 231-238, 2003.

7. Xu, J., Humphrey, P. A., Kibel, A. S., and Song, S. K. Detection and Localization of Prostate Carcinoma and Benign Prostatic Hyperplasia using DTI. Proceedings of the International Society for Magnetic Resonance in Medicine, *12:* 2508, 2004.
8. Xu, J., Humphrey, P. A., Kibel, A. S., Narra, V. R., Ackerman, J. J., and Song, S. K. In vivo Detection and Localization of Prostate Carcinoma using DTI. Proceedings of the International Society for Magnetic Resonance in Medicine, *13:* 2125, 2005.
9. Feinberg, D. A., Hoenninger, J. C., Crooks, L. E., Kaufman, L., Watts, J. C., and Arakawa, M. Inner volume MR imaging: technical concepts and their application. Radiology, *156:* 743-747, 1985.
10. Jeong, E. K., Kim, S. E., Guo, J., Kholmovski, E. G., and Parker, D. L. High-resolution DTI with 2D interleaved multislice reduced FOV single-shot diffusion-weighted EPI (2D ss-rFOV-DWEPI). Magn Reson Med, *54:* 1575-1579, 2005.
11. Xu, J., Naismith, R. T., Trinkaus, K. M., Cross, A. H., and Song, S. K. Towards Accurate In Vivo Diffusion Measurement in Human Optic Nerve. Proceedings of the International Society for Magnetic Resonance in Medicine, *15:* Accepted, 2007.

Appendices

I. "Magnetic Resonance Diffusion Characteristics of Histologically Defined Prostate Cancer in Human" **J. Xu**, P. A. Humphrey, A. S. Kibel, A. Z. Snyder, V. R. Narra, J. J. H. Ackerman, and S. K. Song *Cancer Research*, in preparation

II. "ADC Decrease in Histology Identified Prostate Cancer" **J. Xu**, P. A. Humphrey, A. S. Kibel, A. Z. Snyder, V. R. Narra, and S. K. Song. *Proc. Intl. Soc. Magn. Reson. Med.* **15**, Accepted, 2007

III. "Exclusion of False Positive Identification of Prostate Cancer Using Diffusion Anisotropy" **J. Xu**, P. A. Humphrey, A. S. Kibel, V. R. Narra, and S. K. Song. *Proc. Intl. Soc. Magn. Reson. Med.* **14**, 174, 2006

Appendix I. Magnetic Resonance Diffusion Characteristics of Histologically Defined Prostate Cancer in Humans

Junqian Xu,[1] Peter A. Humphrey,[2] Adam S. Kibel,[3] Abraham Z. Snyder[4,5], Vamsidhar R. Narra,[4] Joseph J. H. Ackerman,[1,4,6] and Sheng-Kwei Song[4]

Departments of [1]Chemistry, [2]Pathology and Immunology, [3]Surgery, [4]Radiology, [5]Neurology, and [6]Internal Medicine, Washington University, One Brookings Drive, St. Louis, MO 63130

RUNNING TITLE
MR Diffusion Characteristics of PCa

KEY WORDS

magnetic resonance (MR), diffusion tensor imaging (DTI), apparent diffusion coefficient (ADC), relative anisotropy (RA), prostate carcinoma (PCa), benign prostatic hyperplasia (BPH), peripheral zone (PZ), central gland (CG).

Grant support: This study was supported, in part, by the Washington University Small Animal Imaging Resource, a National Cancer Institute funded Small Animal Imaging Resource Program facility (R24-CA83060), the Small Animal Imaging Core of the National Cancer Institute (P30 CA91842), the Alvin J. Siteman Cancer Center, the National Science Foundation (P30 NS048056), the U.S. Army Department of Defense Prostate Cancer Research Program (PC050667), and the Midwest Stone Institute.

Note: Preliminary reports of this work may be found in the Proceedings of the International Society for Magnetic Resonance in Medicine, **12**: 2508, 2004, **13**: 2125, 2005, **14**: 174, 2006, and **15**: 5723, 2007.

Requests for reprints: Sheng-Kwei Song, Biomedical MR Laboratory, Department of Radiology, Campus Box 8227, Washington University School of Medicine, 4525 Scott

Avenue, St. Louis, MO 63110. Phone: (314) 362-9988; Fax: (314) 362-0526; E-mail: ssong@wustl.edu.

ABSTRACT

The contrast provided by diffusion sensitive magnetic resonance (MR) in gland confined human prostate cancer (PCa) offers the promise of improved detection and localization. We have previously shown that MR apparent diffusion coefficient (ADC) of PCa in a mouse model is approximately 30% of that in non-cancerous tissues. Here, diffusion tensor imaging (DTI) measurements of PCa were performed *in vivo,* in patients undergoing radical prostatectomy, and *ex vivo,* in the same patients' prostatectomy specimens. For the first time, the imaging data were co-registered to histological sections of the prostatectomy specimens, thereby enabling unambiguous characterization of diffusion parameters in cancerous and benign tissues. Increased cellularity, and thence decreased luminal spaces, in peripheral zone PCa lead to about 40% and 50% ADC decrease compared to benign peripheral zone tissues *in vivo* and *ex vivo*, respectively. In contrast, no significant diffusion anisotropy differences were observed between the cancerous and non-cancerous peripheral zone tissues. The bundled fibromuscular tissues in prostate, such as stromal tissues in benign prostatic hyperplasia (BPH) in central gland, exhibited high diffusion anisotropy. A tissue classification method, combining DTI and T2-weighted image contrasts, provides more specific PCa detection. Using ADC threshold, the PCa identified in volume rendered MR images qualitatively correlate well with histologically determined PCa foci. The diffusion MR results could potentially guide targeted ultrasound biopsy and reduce the false negative rate of random biopsy.

INTRODUCTION

Prostate cancer (PCa) is the leading malignancy and the second most common cause of cancer death in American men (1). Current curative strategies focus on the detection and treatment of early-stage tumors (2). The standard method of diagnosis, transrectal ultrasound guided needle biopsy, misses 20 – 30 % of clinically significant tumors (3). A noninvasive imaging method to accurately localize PCa could guide targeted biopsy and theoretically decrease the false negative rate of needle biopsy. In addition, accurate tumor localization within the prostate would enable recently developed focal therapies, such as cryosurgery, to effect a "partial prostatectomy" (i.e., to ablate just the tumor) (4).

Current magnetic resonance (MR) imaging evaluation of PCa primarily relies on multi-planar T2-weighted (T2w) contrast, which is not sensitive or specific enough for accurate PCa localization (2, 5). Other promising MR methods are being pursued. The ^{1}H MR spectroscopy (MRS) determined citrate to choline resonance intensity ratio has been shown to be a predictive molecular signature of PCa (6). Dynamic contrast enhanced (DCE) MRI has also been explored to evaluate the microvasculature characteristics of PCa, including vascular volume and permeability (7, 8). Both MRS and DCE MRI have been used to complement T2w imaging. However, both methods currently suffer mostly from inadequate image resolution.

Diffusion sensitive MR imaging, with higher resolution than the MRS and DCE MRI, also holds promise for improved PCa localization. The apparent diffusion coefficient (ADC) and relative diffusion anisotropy (RA) of water, parameters derived from diffusion tensor imaging (DTI) reflect tissue microstructure at the micron scale and

hence are sensitive to pathologic changes (9). In an earlier study from this laboratory, the markedly lower ADC of PCa compared to normal prostate provided greatly improved diffusion contrast of PCa *vs.* non-cancerous prostate tissue in a transgenic mouse model *in vivo* (10). The approximately 70% ADC decrease in PCa compared to non-cancerous prostate in the mouse has its origins in the distinct micro-architectural features of these tissues. While there are significant differences between the structure of mouse and human prostate, the characteristic ductal branching morphology of normal prostate tissue and the increased cellularity in PCa are the same. Hence, the distinct micro-architectural features leading to decreased ADC in PCa relative to non-cancerous prostate should also be present in humans.

Indeed, *in vivo* diffusion measurements of human prostate have reported a decreased ADC value in suspected cancerous tissues diagnosed on either T2w images or biopsy results (11-18). While such findings are encouraging, discrepancies in the reported diffusion indices emphasize the circumstantial (inferential) nature of such observations. Remarkably, the expectation of significantly decreased ADC in human PCa *in vivo* has yet to be directly confirmed or quantified *via* "gold standard" PCa identification of the suspected lesions through step-section histology and co-registration. Here, for the first time, the MR diffusion characteristics of histologically defined PCa are directly determined and quantified both *in vivo,* in radical prostatectomy patients prior to surgery, and *ex vivo,* in the same patients' prostatectomy specimens post resection. Quantitatively translating earlier findings in a mouse model (10), this work supports the promise of diffusion sensitive MR for the non-invasive identification and localization of PCa in man.

MATERIALS AND METHODS

Patients: Twenty four patients undergoing radical prostatectomy (mean age 62 years; range 46 - 76 years) who had not received any preoperative treatment such as androgen ablation or radiation therapy were recruited for this study, which was approved by the local Institutional Review Board. Informed consent was obtained from each patient prior to the study. The prostates of 14 patients, of which 12 had significant tumor burden (> 5%), were examined both *in vivo*, prior to surgery, and *ex vivo*, after resection. The prostates of the other 10 patients, of which 4 had significant tumor burden (> 5%), were examined only *ex vivo*, after resection. The 16 patients with post-surgery histology determined significant tumor burden (mean volume 20%, range 5% - 46%) had a median post-resection Gleason score of 3 + 4 = 7 (range 3 + 3 = 6 to 4 + 5 = 9). Nine of the 16 patients had peripheral zone (PZ) PCa invading the central gland (CG) or PCa originating from the transitional zone (TZ).

***In vivo* MRI:** Fourteen of the patients underwent DTI and conventional T2w MR imaging before surgery. *In vivo* imaging was performed on a 1.5 tesla MR scanner (Sonata, Siemens AG, Erlangen, Germany) using a four-channel body phased-array surface coil. The whole prostate gland was examined, employing both diffusion weighted (DW) and T2w multislice (2.5 mm thick transverse slices) imaging. DWI were performed using a single shot spin-echo echo planar imaging (SE-EPI) sequence with field of view (FOV) 256 × 256 mm^2, data matrix 128 × 128, partial *k*-space 6/8, TR/TE 4000/76 ms. An acceleration factor of two was achieved in the phase encoding direction *via* the generalized auto-calibrating partially parallel acquisition (GRAPPA) technique

(19). Four image datasets, each consisting of one image with *b* value of 0 s/mm^2 and six diffusion sensitized images on six non-collinear (oblique dual gradient or ODG) diffusion encoding directions with b values of 500 s/mm^2, were acquired and the magnitude images averaged (20). Sixteen of these averaged full DWI data sets, each post-processed to correct for artifacts resulting from eddy currents and motion, were collected and averaged to further improve the signal-to-noise ratio (SNR) (21). ADC and scaled relative anisotropy (sRA) or A_σ maps were calculated on a pixel-by-pixel basis after linear least square fitting of the diffusion signal decay curve and diffusion tensor matrix diagonalization (9). T2w images were acquired with a turbo spin echo (TSE) sequence with FOV 256 × 256 mm^2, matrix 256 × 256, echo train length (ETL) 13, and TR/TE 2800/120 ms.

***Ex vivo* MRI:** After surgery, each prostate specimen was fixed with 10% formalin in phosphate buffered saline (PBS, pH = 7.4) for more than 48 hours. The specimen was step-sectioned at 4 mm intervals from base to apex using a laboratory designed and constructed prostate slicer. The step-sectioned slices were re-grouped into a whole prostate with thin plastic spacers placed between each 4 mm slice. The regrouped prostate specimens then were wrapped in a lint-free tissue (Kimwipes, Kimberly-Clark, GA) and placed in a formalin filled plastic bag to hold the slices in place and to prevent tissue dehydration. *Ex vivo* specimens were imaged on a 4.7-tesla MR scanner (console by Varian NMR Systems, Palo Alto, CA; magnet by Oxford Instruments, Oxford, UK; gradients by Magnex Scientific, Oxford, UK) using a 5-cm diameter quadrature "Litzcage" radio frequency coil (Doty Scientific, Columbia, SC). A mutislice spin echo imaging sequence with a pair of diffusion sensitizing pulsed gradients

was employed to acquire DW images (22). High resolution (500 × 500 × 500 μm) images were collected with diffusion time (Δ) 12 ms, diffusion gradient duration (δ) 4 ms, slice thickness 0.5 mm, FOV 6.5 cm × 6.5 cm, data matrix 128 × 128, TR/TE 6000/35ms. A sufficient number of slices were obtained to cover each specimen completely. Eight DW image datasets, each consisting twelve images with two *b* values of 45 and 1130 s/mm^2 on six non-collinear (oblique dual gradient or ODG) diffusion encoding directions, were averaged in the complex *k*-space (20). Then the magnitude images were used to calculate ADC and sRA maps by standard procedures as for the *in vivo* experiemnts (9). T2w images were acquired with a multi-slice SE sequence with FOV 6.5 × 6.5 mm^2, data matrix 128 × 128, and TR/TE 5000/60 ms.

Histology: After *ex vivo* MRI data was acquired, each 4 mm slice from the resected specimen was cut into halves or into quarters depending on the size of each slice and embedded in paraffin. A thin 4-μm thick slice was obtained parallel to the MR imaging plane for hematoxylin and eosin (H & E) staining. Regions of PCa and benign prostatic hyperplasia (BPH) were delineated in blue/black and red, respectively, on all H & E stained slides by an experienced urologic pathologist (P.A.H) blind to the MR imaging results. The intraglandular tumor extent, reported as volume percentage of the gland containing carcinoma, was determined by grid morphometry (23). Histology slides from half-cut or quarter-cut specimens were later digitized and fused together into whole cross-sectional slices.

MR/Histology Image Co-Registration: The specifically sliced prostatectomy specimens maintain near identical coordinate systems between *ex vivo* diffusion MR and histology. To account for histological slicing and mounting distortions, a two-

dimensional (2D) thin plate spline (TPS) warping with twelve degrees of freedom (DOF) was performed using 10 – 20 control points to correct the histology image coordinates to the coordinates of *ex vivo* MR images using ImageJ (NIH, Bethesda, MD) software. Using a rigid body three-dimensional (3D) affine transformation with nine DOF, each *ex vivo* ADC and sRA maps were further transformed into the coordinates of the respective *in vivo* T2w image based on the manual alignment of intragladular structures using the ITK registration module in Analyze (Mayo Clinic, Rochester, MN) software. The final step of co-registering the *in vivo* ADC and sRA maps to the *in vivo* T2w images were accomplished by using an unsupervised 3D affine transformation with twelve DOF with laboratory developed software (21). As summarized in Fig. 1, a match of alignment (orientation and position) between histology slides and *in vivo* ADC and sRA slices in the standard *in vivo* T2w image space was achieved for purposes of mapping the histologically identified tissue types onto the *in vivo* MR images. In eight patients with minimum tumor burden (< 5%), it was not possible to reliably map cancerous tissue regions from histology to MR images, leaving 16 *ex vivo* and 12 *in vivo* cases on which basis to define histology-DTI PCa correspondence.

Statistical Analysis: Paired student *t*-tests were performed to compare mean ADC and sRA between cancerous and benign PZ tissues with n = 16 and 12 for *ex vivo* and *in vivo*, respectively. Results are presented as mean ± standard deviation (SD). Statistical significance was defined as $p < 0.01$.

Volume Rendering: Representative *ex vivo* and *in vivo* DTI images were volume rendered using Amira (Mercury Computer Systems, Richmond, TX) software. The whole prostate gland was segmented from *ex vivo* or *in vivo* T2w images. The ADC and

sRA values were imported into yellow-orange and green-blue channels, respectively. The scales for ADC were inverted. Hence, bright yellow-orange regions in the MR images were identified as carcinoma determined by an upper ADC threshold (mean tumor ADC + SD). The scales for sRA were chosen for optimal visualization of fibromuscular tissues. For *ex vivo* cases, two dimensional (2D) projection images were taken and ejaculatory ducts were segmented from ADC map separately due to the very high ADC value of the structure (color scale reversed comparing with the prostate tissues). For *in vivo* cases, the volume rendered images were projected onto representative T2w images.

Results

After MR and histology image co-registration for each slice, the PCa region and the benign tissue region in the PZ were translated from the histology slide (Fig. 2E) to both the *ex vivo* (Fig. 2D) and *in vivo* ADC maps (Fig. 2A). The ADC value of PCa tissue (0.43 ± 0.06 μm^2/ms *ex vivo*, Fig. 2D blue arrow, and 0.90 ± 0.13 μm^2/ms *in vivo*, Fig. 2A blue arrow) was significantly lower than that of the non-cancerous PZ tissues (0.99 ± 0.16 μm^2/ms *ex vivo*, and 1.66 ± 0.21 μm^2/ms *in vivo*). Microscopically, normal prostate has a branching duct-acinar glandular architecture embedded in a dense fibromuscular stroma (Fig. 2G). This duct-acinar structure underlies the diffusion MR characteristics of the prostate gland in both human and the previously reported mouse model. In prostate carcinoma, tightly packed tumor cells disrupt the duct-acinar structure leading to decreased ADC in tumor due to the cellularity induced diffusion restriction (Fig. 2H).

The water molecule in dense fibromuscular stroma in the prostate may exhibit high diffusion anisotropy as it diffuses in and between the smooth muscle cells preferentially along the length of the cells. However, this microscopic diffusion anisotropy is not particularly evident in the PZ with the *b* values and scale of the MR imaging resolution employed herein (Fig. 2F, Fig. 3C and Fig. 4D, PZ tissues). Indeed, a relatively low diffusion anisotropy was observed in the PZ (sRA = 0.13 ± 0.05 and 0.06 ± 0.03 for *ex vivo* and *in vivo* determinations, respectively). The low diffusion anisotropy in the PZ likely reflects the random orientation of fibromuscular cells in the PZ (Fig. 2G and H). Importantly, no significant diffusion anisotropy differential was observed (peripheral zone, Fig. 2C and F, Fig. 3A and C) between the cancerous and non-cancerous PZ tissues (sRA = 0.13 ± 0.04 *vs.* 0.13 ± 0.03, $p = 0.89$ for *ex vivo*; and sRA = 0.08 ± 0.02 *vs.* 0.05 ± 0.02, $p = 0.012$ for *in vivo*). However, when the fibromuscular cells are bundled together at a length scale comparable to MRI voxel dimensions (Fig. 2I), higher diffusion anisotropy (sRA = 0.34 ± 0.08 *ex vivo* and 0.13 ± 0.06 *in vivo*) in those regions becomes distinctive and distinguishable (red arrows, Fig. 2C and F, Fig. 3A and C, and Fig. 4 D) from that in the glandular region.

The appearance of BPH in ADC map (Fig. 4E) or T2w image (Fig. 4F) is very heterogeneous, reflecting the complicated BPH tissue composition. BPH regions with both ADC and T2w hypointensity could mimic PCa in the CG (Fig. 1A and B, red arrows), leading to false positive PCa identification. The high diffusion anisotropy in the bundled fibromuscular cells provides a unique contrast for differentiating these BPH nodules from PCa (Fig. 2C and F). Notably, the high diffusion anisotropy appears not only in the stromal components within BPH, but also in the fibrous tissues surrounding

the BPH (Fig. 4D), as the expanding BPH nodule pushes and compacts the fibromuscular tissue network around it. This high diffusion anisotropy pattern surrounding the BPH was best visualized in the volume rendered DTI images (Fig. 4B).

A prostate tissue classification method was proposed combining both DTI and T2w contrasts (Table 1). The various tissue types were verified by histological analysis after co-registration. In general, ADC contrast parallels the T2w contrasts with ADC being more specific than T2w contrast for PZ PCa (Fig. 2A, B white arrows). The diffusion anisotropy (sRA) provides a unique contrast to differentiate PCa from stromal BPH in the CG, while its usage for PZ PCa is limited.

To take advantage of the DTI contrasts quantitatively, six representative cases with different tumor burden are presented in Figs. 4 and 5 for *ex vivo* and *in vivo*, respectively. The tumor volume and distribution were highlighted in bright orange in the volume rendered and projected DTI images using ADC threshold (mean tumor ADC + SD) and color coding, which correlate well with the corresponding histologically defined extent and stage for the same tumors.

Discussion

The luminal space in benign human prostate is, on average, hundreds of microns wide. Under conditions of typical diffusion sensitive MR imaging protocols as in this study with an *in vivo* diffusion time Δ of 30 ms, it is estimated that water diffuses over a distance of tens of microns. Thus, water in the normal prostate is relatively unrestricted and the ADC measured *in vivo* in humans is fairly high, typically ~ 1.7 $\mu m^2/ms$. (Note: human brain grey or white matter has ADC of ~ 0.8 $\mu m^2/ms$ *in vivo*.) The high

cellularity of most PCa presents hindrances and restrictions to water diffusion over a distribution of length scales covering from the submicron to tens of microns range. This is the displacement scale to which the MR diffusion imaging is sensitive. Thus, the majority of PCa is found to have a markedly lower ADC *in vivo* than non-cancerous prostate. It is noteworthy that some medium grade (e.g., Gleason score = 3) infiltrative PCa does not affect the prostate cellularity, hence theoretically no change in ADC may be expected. This type of PCa may also be of significant clinical relevance and require other contrast mechanisms or modality to detect.

The nearly two fold *in vivo* ADC difference between PCa and benign prostate was preserved in formalin-fixed prostatectomy specimens, also observed by Williams *et al*. (24). Although the formalin fixation process reduces the ADC's for both PCa and normal prostate tissue, the microstructure is largely preserved as evidenced by the comparable ADC decrease observed for PCa relative to normal prostate tissue both *in vivo* (~ 40%) and *ex vivo* (~ 50%). We speculate that further diffusion sensitive MR studies of radical prostatectomy specimens may provide a correlation between tumor grade and certain MR diffusion signature, which can be translated to *in vivo* studies.

The ADC value in the human prostate gland is no homogeneous (Fig. 2D). In normal peripheral zone tissues, ADC maps acquired *ex vivo* usually display bright spots (high ADC values) scattered throughout a relatively uniform background of somewhat lower ADC. We speculate that these high ADC voxels reflect regions with large diameter glandular spaces. This ADC heterogeneity is lost due to significant partial volume effect and hence not observed under the coarser MR spatial resolution obtained *in vivo* (Fig. 2A).

The ADC distribution is even more heterogeneous in the CG, including the transition zone, spanning the complete spectrum of observable ADC values in the prostate (Fig. 4E). The variation in stromal and epithelial tissue composition, the presence of BPH, and the formation of cysts in the CG all contribute to the observed wide distribution of ADC values. Regions of BPH composed of compact fibromuscular stroma exhibit low ADC values. In optical density measurements, these stromal BPH appears to be similar in tissue density to the closely packed glands in PCa (25). This is likely the cause of the overlap of ADC values between PCa and BPH. On the other hand, BPH dominated by glandular epithelial cell proliferation exhibits heterogeneous ADC contrast. Regions of sparse epithelial BPH components exhibit relatively high ADC values comparable to begin PZ tissues, while regions of compact epithelial BPH components exhibit considerably low ADC values similar to PCa. Therefore, the overall BPH ADC-contrast depends on the ratio of the stromal and epithelial components, as well as the compactness of cell packing. As the composition of BPH and CG is extremely variable and almost always heterogeneous, ADC contrast will vary significantly between different regions in the same patient's prostate and between patients. Although such variation is less obvious *in vivo* than *ex vivo* due to increased partial volume averaging at the lower MR spatial resolution of *in vivo* images, using only mean ADC value to describe BPH or CG in general is likely to provide little information and could be misleading.

The network of fibromuscular connective tissues in the prostate leads to the observed diffusion anisotropy. Relatively high anisotropy is commonly observed *ex vivo* in the periurethral muscles, anterior fibromuscular regions, stromal BPH or fibrous

tissues surrounding the BPH. The latter develops as the expanding BPH pushes and tightens the fibromuscular system around it (Fig. 4D). Stromal BPH in the CG usually displays similar ADC and T2w contrast as PCa (Fig. 1A and B, red arrow), likely due to the similar tissue density (25). In such ambiguous cases, the contrast provided by diffusion anisotropy may offer a means of differentiating BPH from PCa in the central gland, which accounts for about 30 % of the PCa occurrence.

The microscopic anisotropy is subject to partial volume averaging. Hence, much lower diffusion anisotropy is found for images acquired *in vivo* (resolution $2 \times 2 \times 2.5$ mm^3) comparing to that *ex vivo* (resolution $0.5 \times 0.5 \times 0.5$ mm^3). The diffusion anisotropy measurement, reporting the standard deviation of the principal diffusivities, is also sensitive to measurement noise. Indeed, a lower limit of observed anisotropy is determined by the SNR. As SNR is always a concern for the *in vivo* diffusion imaging experiment, artifactually high diffusion anisotropy due to noise variation is not uncommon (Fig. 2C blue arrow). This is especially true in the PCa region where short T2 leads to the reduced SNR (26). Microscopically, there is no histological evidence to support an increased density of fibromuscular tissues in PCa. In addition, the fibromuscular cells in PCa, like those in the benign peripheral zone tissues, do not bundle together or show a coherent orientation (Fig. 2H). Such random micro-architecture is unlikely to contribute to result in the increased diffusion anisotropy under the present imaging conditions. Indeed, we did not observe a significant anisotropy differential between the PCa and non-PCa peripheral zone tissues, either *ex vivo* or *in vivo*. This latter negative finding is in contrast to the positive results reported by Gibbs *et al.* and the preliminary findings on pre and post hormone/radiation therapy PCa patients by

Vigneron *et al.* and Chen *et al.*, respectively, where significant anisotropy contrast between these tissues were reported (18, 27, 28). Sinha *et al.* reported even higher values of anisotropy (mean sRA range 0.40 - 0.46) for both the peripheral zone and central gland tissue in a study of volunteers (29). Although age differences could be a confounding factor, such high diffusion anisotropy is likely due to artifactual noise variation, as reported by Reinsberg *et al.* evaluating effect of SNR on diffusion anisotropy (30). The low diffusion anisotropy of PCa and non-PCa peripheral zone tissues reported in the present study are in agreement with the preliminary reports by Reinsberg *et al.* using a EPI diffusion sequence, Hacker *et al.* and Roebuck *et al.* using a line-scan diffusion sequence, and Vigneron *et al.* using a fast spin-echo diffusion sequence (28, 30-32). Considering the technical limitations for *in vivo* body diffusion imaging, accurate diffusion anisotropy measurement in human prostate *in vivo* will likely remain to be a challenge.

The precise co-registration using hisgologically identified PCa employed in this study avoids the uncertainty of *in vivo* T2w image ROI placement and/or the sampling error of needle biopsy. Such methodological differences likely explain the approximately 30% lower *in vivo* PCa mean ADC value (0.99 $\mu m^2/ms$) reported herein compared to that reported for suspected PCa by others (range 1.27 - 1.43 $\mu m^2/ms$) (16). Admittedly co-registration error is a concern in our study, especially the manual registration step used to translate the *ex vivo* coordinates to the *in vivo* space. Nevertheless, the patients recruited in this study (mean age 62 years) commonly harbor large amounts of BPH, cysts and thickened periurethera connective muscle tissue. These intraglandular landmarks, easily identified in both *in vivo* T2w image, and *ex vivo* ADC or sRA map, facilitating the

manual co-registration procedure. Such landmarks also help to guide the placement of control points in both histology slide and *ex vivo* MR images to achieve an accurate warping of the histology slide into the *ex vivo* MR coordinate. The latter could be performed more accurately using whole mount histology slides. Additionally, the whole co-registration procedure could be optimized by using mutual information based automatic procedures such as that reported by Meyer *et al.* (33).

In summary, we report herein the diffusion properties – ADC and anisotropy – for histologically defined PCa *in vivo* and *ex vivo*. The good correlation between histology and volume rendered *in vivo* and *ex vivo* diffusion images suggests that the ADC threshold may provide a means for PCa volume estimation and tumor staging in peripheral zone tissue. Exploiting indices such as ADC and diffusion anisotropy is a valuable complement to conventional T2w imaging of the prostate.

Acknowledgments

The authors appreciate the assistances in patient recruitment and coordination by Aleksandra Klim and Kelly Granda and the MR scanner technical support by Glenn Foster.

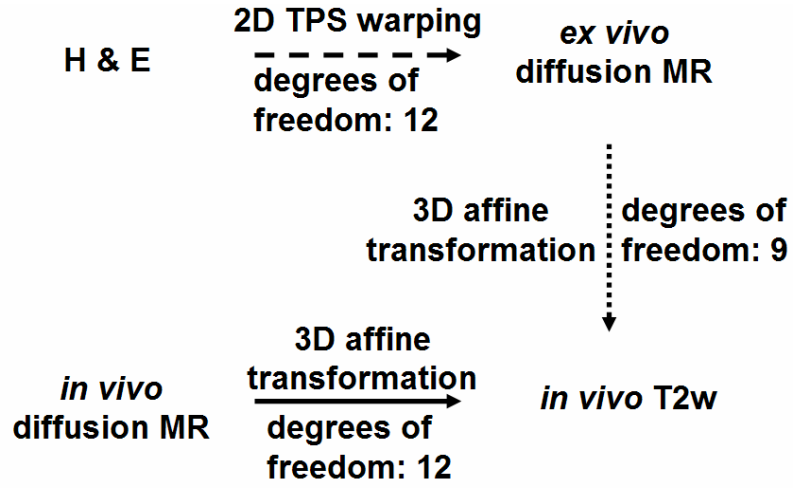

Figure 1. Overview of histology and MR co-registration scheme. The dashed line represents the semi-automatic thin plate spline (TPS) warping procedure using manually placed control points. The dotted line represents the manual image registration procedure to transform *ex vivo* coordinates into *in vivo* T2w coordinates. The solid line represents the unsupervised *in vivo* image co-registration procedure.

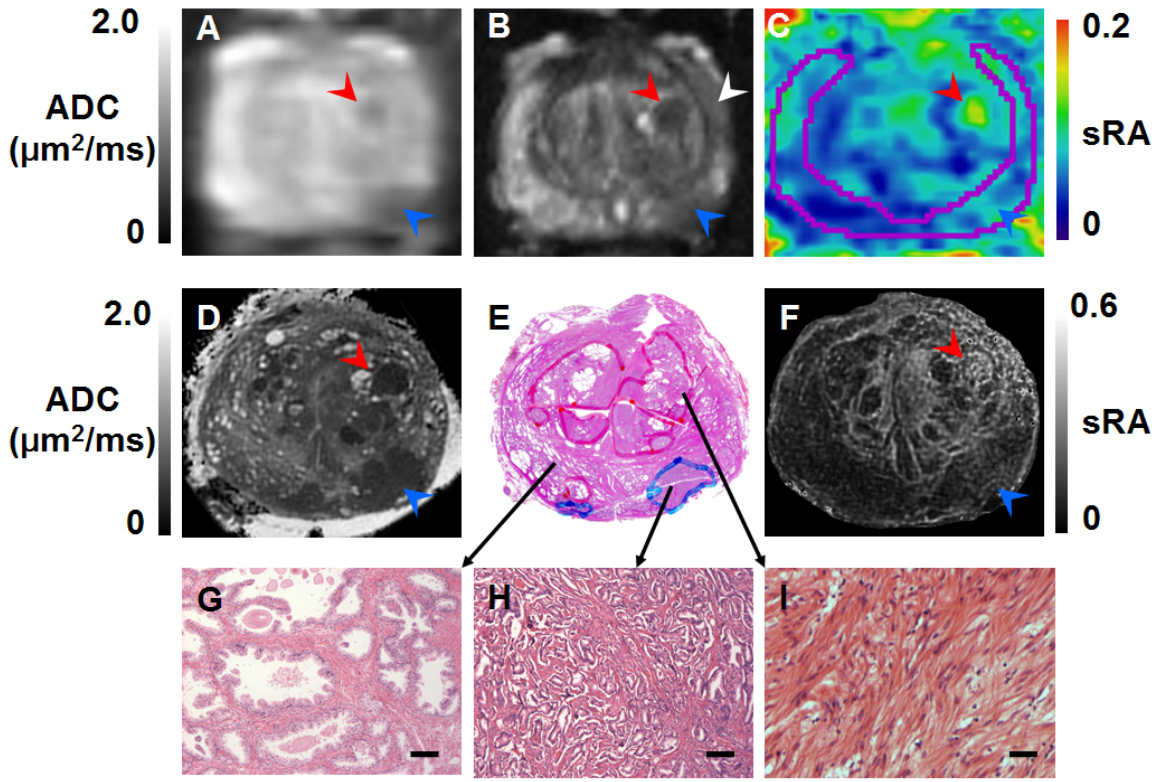

Figure 2. Co-registered images illustrate the tissue microstructure underpinning the MR diffusion characteristics. A) *in vivo* ADC, B) *in vivo* T2w, C) *in vivo* color coded sRA, D) *ex vivo* ADC, E) H & E slide, and F) *ex vivo* sRA. The cancerous and BPH regions in the H & E slide were marked in blue and red, respectively, by a urologic pathologist. Blue and red arrows indicate regions of PCa and stromal BPH, respectively, as diagnosed by histology. The white arrow in panel B indicates a T2 hypointense region that could be mistaken for PCa without the additional co-registered diffusion data. The peripheral zone were delineated in panel B and mapped onto panel C in magenta. High resolution H & E examinations reveal the micro-structures of different types of tissues in G) benign peripheral zone, H) PCa, and I) stromal BPH (10× magnification, scale bar = 100 μm).

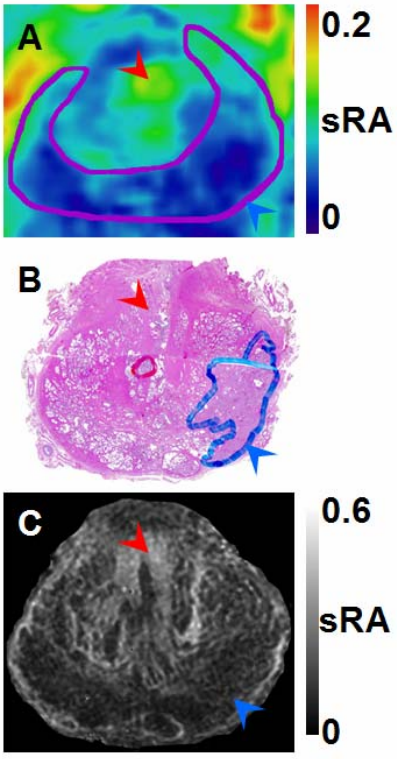

Figure 3. One representative case illustrates the lack of diffusion anisotropy differential between normal and cancerous tissue in the peripheral zone. The cancerous and BPH regions in the H & E slides were marked in blue and red, respectively, by a urologic pathologist. Red and blue arrows indicate regions of fibromuscular and carcinoma tissues, respectively, as identified by histology. (A) *in vivo* sRA map, (B) H & E slide, and (C) *ex vivo* sRA map. The magenta line in B delineates the peripheral zone as in Fig. 2.

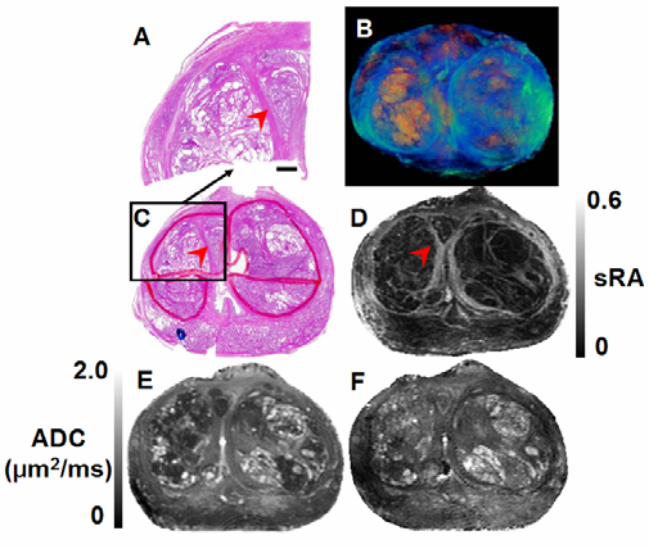

Figure 4. One representative case illustrates the diffusion anisotropy delineating the BPH in prostate. The cancerous and BPH regions in the H & E slides were marked in blue and red, respectively, by a urologic pathologist. The BPH was largely composed of epithelial nodules with variable size and compactness. Red arrows indicate regions of bundled fibromuscular tissues, respectively, as identified by histology. (A) magnified (scale bar = 3 mm) right anterior quadrant of the H & E slide, (B) 3D reconstructed *ex vivo* DTI image (image scale detailed in Fig. 5), (C) H & E slide, (D) *ex vivo* sRA map, (E) *ex vivo* ADC map, (F) *ex vivo* T2w image.

		ADC	sRA	T2w
PZ	PCa	hypo	iso	hypo
	Benign	-	-	-
CG	PCa	hypo	iso	hypo
	Stromal BPH	hypo	hyper	hypo
	Epithelial BPH	hetero	iso	hetero
	Benign	-	-	-

Table 1. Tissue type classification combining DTI and T2w contrasts. Benign tissues (-) in PZ and CG, respectively, were used as benchmarks for MR contrasts. MR image contrasts were listed as hypo(intense), iso(intense), hyper(intense) or hetero(geneous).

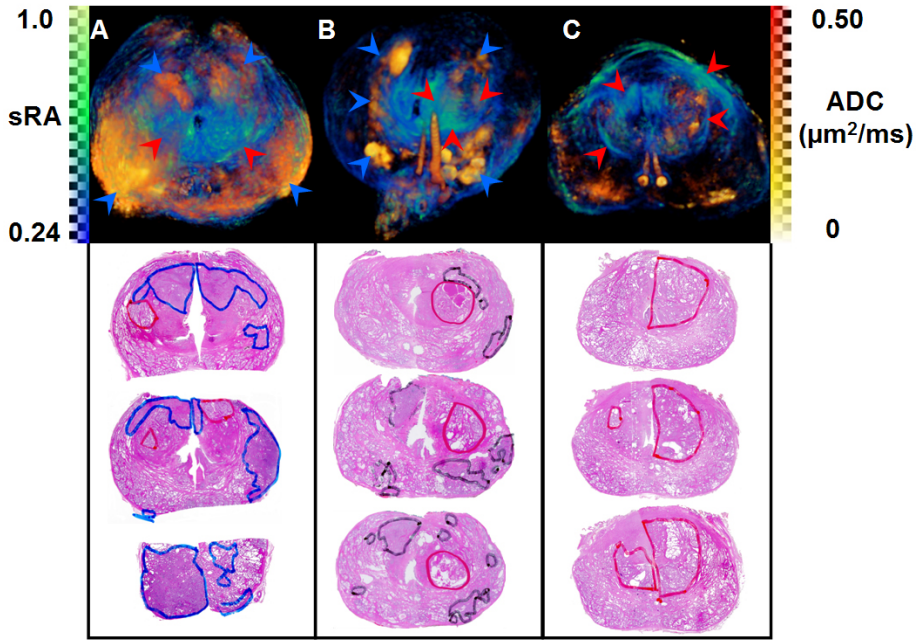

Figure 5. Representative specimens with different tumor sizes demonstrate good pathologic correlation between *ex vivo* DTI and histology. 3D reconstructed *ex vivo* DTI images (top row, projected view in 2D) were co-registered with step-section histology in three representative specimens (each column) of histologically defined PCa extents and stages (A) 40% T3b, (B) 16% T2c, and (C) 4% T2c. The cancerous and BPH regions in the H & E slides were marked in blue and red, respectively, by a urologic pathologist. In the MR images, the ADC and diffusion anisotropy values were imported into the yellow-orange and green-blue channels, respectively. Bright yellow-orange regions in the MR images were identified as carcinoma determined by ADC threshold (*ex vivo* PCa mean ADC + SD). Red and blue arrows indicate regions of fibromuscular and carcinoma tissues, respectively, as identified by histology and their co-registered diffusion contrast in the MR images. Pairs of ejaculatory ducts with high ADC value (color scale irrelevant, obvious in B and C) are segmented from ADC map seperately. The empty urethra lumen resides in the middle of each image.

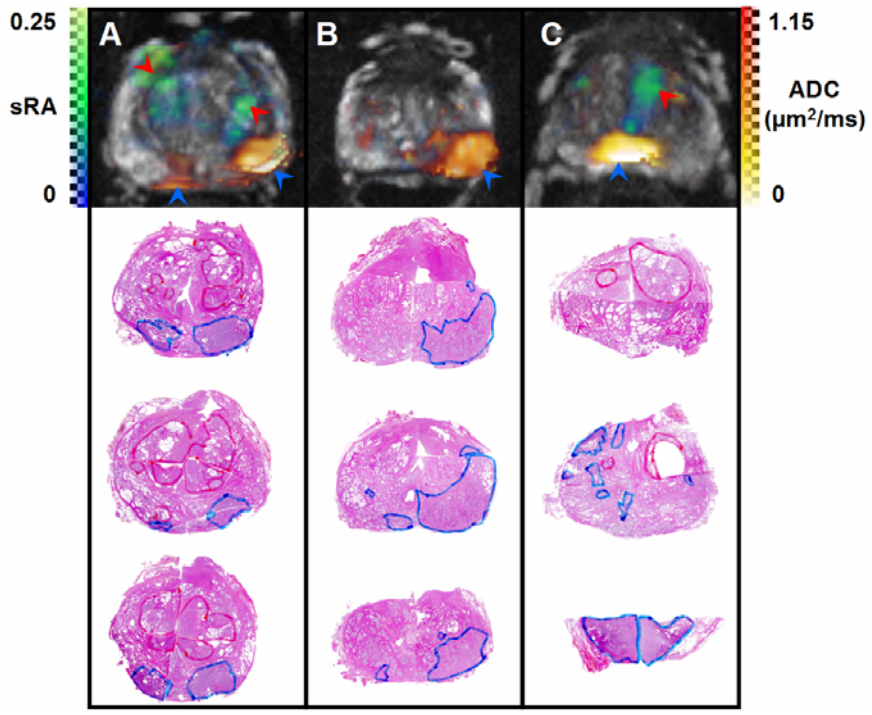

Figure 6. Representative specimens with different tumor sizes demonstrate good pathologic correlation between *in vivo* DTI and histology. 3D reconstructed *in vivo* DTI images (top row, projected onto a representative T2w image) were co-registered with step-section histology in three representative specimens (each column) of histologically defined PCa extents and stages (A) 15% T3a, (B) 40% T3a, and (C) 20% T3a. The cancerous and BPH regions in the H & E slides were marked in blue and red, respectively, by a urologic pathologist. In the MR images, the ADC and diffusion anisotropy values were imported into the yellow-orange and green-blue channels, respectively. Bright yellow-orange regions in the MR images were identified as carcinoma determined by ADC threshold (*in vivo* PCa mean ADC + SD). Red and blue arrows indicate regions of fibromuscular and carcinoma tissues, respectively, as identified by histology and their co-registered diffusion contrast in the MR images.

1. Jemal, A., Siegel, R., Ward, E., Murray, T., Xu, J., Smigal, C., and Thun, M. J. Cancer statistics, 2006. CA Cancer J Clin, *56:* 106-130, 2006.
2. Kantoff, P. W., Rarroll, P. R., and D'Amico, A. V. (eds.) Prostate Cancer: Principles & Practice, 1st edition, p. 278-280. Philadelphia: Lippincontt Williams & Wilkins, 2002.
3. Keetch, D. W., Catalona, W. J., and Smith, D. S. Serial prostatic biopsies in men with persistently elevated serum prostate specific antigen values. J Urol, *151:* 1571-1574, 1994.
4. Katz, A. E. and Rewcastle, J. C. The current and potential role of cryoablation as a primary therapy for localized prostate cancer. Curr Oncol Rep, *5:* 231-238, 2003.
5. Coakley, F. V., Qayyum, A., and Kurhanewicz, J. Magnetic resonance imaging and spectroscopic imaging of prostate cancer. J Urol, *170:* S69-75; discussion S75-66, 2003.
6. Kurhanewicz, J., Swanson, M. G., Nelson, S. J., and Vigneron, D. B. Combined magnetic resonance imaging and spectroscopic imaging approach to molecular imaging of prostate cancer. J Magn Reson Imaging, *16:* 451-463, 2002.
7. Padhani, A. R., Gapinski, C. J., Macvicar, D. A., Parker, G. J., Suckling, J., Revell, P. B., Leach, M. O., Dearnaley, D. P., and Husband, J. E. Dynamic contrast enhanced MRI of prostate cancer: correlation with morphology and tumour stage, histological grade and PSA. Clin Radiol, *55:* 99-109, 2000.
8. Engelbrecht, M. R., Huisman, H. J., Laheij, R. J., Jager, G. J., van Leenders, G. J., Hulsbergen-Van De Kaa, C. A., de la Rosette, J. J., Blickman, J. G., and Barentsz, J. O. Discrimination of prostate cancer from normal peripheral zone and central gland tissue by using dynamic contrast-enhanced MR imaging. Radiology, *229:* 248-254, 2003.
9. Basser, P. J. and Pierpaoli, C. Microstructural and physiological features of tissues elucidated by quantitative-diffusion-tensor MRI. J Magn Reson B, *111:* 209-219, 1996.
10. Song, S. K., Qu, Z., Garabedian, E. M., Gordon, J. I., Milbrandt, J., and Ackerman, J. J. Improved magnetic resonance imaging detection of prostate cancer in a transgenic mouse model. Cancer Res, *62:* 1555-1558, 2002.
11. Gibbs, P., Tozer, D. J., Liney, G. P., and Turnbull, L. W. Comparison of quantitative T2 mapping and diffusion-weighted imaging in the normal and pathologic prostate. Magn Reson Med, *46:* 1054-1058, 2001.
12. Issa, B. In vivo measurement of the apparent diffusion coefficient in normal and malignant prostatic tissues using echo-planar imaging. J Magn Reson Imaging, *16:* 196-200, 2002.
13. Chan, I., Wells, W., 3rd, Mulkern, R. V., Haker, S., Zhang, J., Zou, K. H., Maier, S. E., and Tempany, C. M. Detection of prostate cancer by integration of line-scan diffusion, T2-mapping and T2-weighted magnetic resonance imaging; a multichannel statistical classifier. Med Phys, *30:* 2390-2398, 2003.

14. Hosseinzadeh, K. and Schwarz, S. D. Endorectal diffusion-weighted imaging in prostate cancer to differentiate malignant and benign peripheral zone tissue. J Magn Reson Imaging, *20:* 654, 2004.
15. Sato, C., Naganawa, S., Nakamura, T., Kumada, H., Miura, S., Takizawa, O., and Ishigaki, T. Differentiation of noncancerous tissue and cancer lesions by apparent diffusion coefficient values in transition and peripheral zones of the prostate. J Magn Reson Imaging, *21:* 258-262, 2005.
16. Pickles, M. D., Gibbs, P., Sreenivas, M., and Turnbull, L. W. Diffusion-weighted imaging of normal and malignant prostate tissue at 3.0T. J Magn Reson Imaging, *23:* 130-134, 2006.
17. Kozlowski, P., Chang, S. D., Jones, E. C., Berean, K. W., Chen, H., and Goldenberg, S. L. Combined diffusion-weighted and dynamic contrast-enhanced MRI for prostate cancer diagnosis--correlation with biopsy and histopathology. J Magn Reson Imaging, *24:* 108-113, 2006.
18. Gibbs, P., Pickles, M. D., and Turnbull, L. W. Diffusion imaging of the prostate at 3.0 tesla. Invest Radiol, *41:* 185-188, 2006.
19. Griswold, M. A., Jakob, P. M., Heidemann, R. M., Nittka, M., Jellus, V., Wang, J., Kiefer, B., and Haase, A. Generalized autocalibrating partially parallel acquisitions (GRAPPA). Magn Reson Med, *47:* 1202-1210, 2002.
20. Hasan, K. M., Parker, D. L., and Alexander, A. L. Comparison of gradient encoding schemes for diffusion-tensor MRI. J Magn Reson Imaging, *13:* 769-780, 2001.
21. Shimony, J. S., Burton, H., Epstein, A. A., McLaren, D. G., Sun, S. W., and Snyder, A. Z. Diffusion tensor imaging reveals white matter reorganization in early blind humans. Cereb Cortex, *16:* 1653-1661, 2006.
22. Stejskal, E. O. and Tanner, J. E. Spin diffusion measurements: spin echoes in the presence of a time-dependent field gradient. J. Chem. Phys., *42:* 288-292, 1965.
23. Humphrey, P. A. and Vollmer, R. T. Intraglandular tumor extent and prognosis in prostatic carcinoma: application of a grid method to prostatectomy specimens. Hum Pathol, *21:* 799-804, 1990.
24. Williams, M. C., Does, M. D., and Price, R. R. ADC Mapping of Whole Excised Human Prostate. Proceedings of the International Society for Magnetic Resonance in Medicine, *12:* 2064, 2004.
25. Quint, L. E., Van Erp, J. S., Bland, P. H., Del Buono, E. A., Mandell, S. H., Grossman, H. B., and Gikas, P. W. Prostate cancer: correlation of MR images with tissue optical density at pathologic examination. Radiology, *179:* 837-842, 1991.
26. Liney, G. P., Turnbull, L. W., Lowry, M., Turnbull, L. S., Knowles, A. J., and Horsman, A. In vivo quantification of citrate concentration and water T2 relaxation time of the pathologic prostate gland using 1H MRS and MRI. Magn Reson Imaging, *15:* 1177-1186, 1997.
27. Chen, A. P., Xu, D., Henry, R., Qayyum, A., Kurhanewicz, J., and Vigneron, D. B. Diffusion Tensor Imaging of the Prostate Following Therapy. Proceedings of the International Society for Magnetic Resonance in Medicine, *11:* 579, 2003.
28. Vigneron, D. B., Xu, D., Chen, A. P., Swanson, M. G., and Kurhanewicz, J. Diffusion Tensor Imaging of the Prostate using Single-Shot Fast Spin Echo.

Proceedings of the International Society for Magnetic Resonance in Medicine, *10:* 457, 2002.

29. Sinha, S. and Sinha, U. In vivo diffusion tensor imaging of the human prostate. Magn Reson Med, *52:* 530-537, 2004.
30. Reinsberg, S. A., Brewster, J. M., Payne, G. S., Leach, M. O., and deSouza, N. M. Anisotropic Diffusion in Prostate Cancer: Fact or Artefact? Proceedings of the International Society for Magnetic Resonance in Medicine, *13:* 269, 2005.
31. Haker, S. J., Szot Barnes, A., Maier, S. E., Tempany, C. M., and Mulkern, R. V. Diffusion Tensor Imaging for Prostate Cancer Detection: Preliminary Results from a Biopsy-Based Assessment. Proceedings of the International Society for Magnetic Resonance in Medicine, *13:* 2126, 2005.
32. Roebuck, J. R., Haker, S. J., Tempany, C. M., Rybicki, F. J., Maier, S. E., and Mulkern, R. V. Diffusion Tensor Imaging of the Prostate: Low Anisotropies in Central Gland and Peripheral Zone in Men with Adenocarcinoma. Proceedings of the International Society for Magnetic Resonance in Medicine, *14:* 3338, 2006.
33. Meyer, C. R., Moffat, B. A., Kuszpit, K. K., Bland, P. L., McKeever, P. E., Johnson, T. D., Chenevert, T. L., Rehemtulla, A., and Ross, B. D. A methodology for registration of a histological slide and in vivo MRI volume based on optimizing mutual information. Mol Imaging, *5:* 16-23, 2006.

ADC Decrease in Histology Identified Prostate Cancer

J. G. Xu[1], P. A. Humphrey[2], A. S. Kibel[3], A. Z. Snyder[4,5], V. R. Narra[4], and S-K. Song[4]

[1]Chemistry, Washington University in St. Louis, St. Louis, MO, United States, [2]Pathology & Immunology, Washington University in St. Louis, St. Louis, MO, United States, [3]Surgery, Washington University in St. Louis, St. Louis, MO, United States, [4]Radiology, Washington University in St. Louis, St. Louis, MO, United States, [5]Neurology, Washington University in St. Louis, St. Louis, MO, United States

Introduction

The ability to accurately localize prostate carcinoma (PCa) within prostate gland non-invasively can dramatically improve PCa diagnosis and treatment. However, conventional T2 weighted (T2W) imaging has not proven sensitive or specific enough to localize gland-confined PCa. Recently substantial decrease of mean water apparent diffusion coefficient (ADC), due to disruption of the prostate ductal structures by PCa, provides a unique contrast for tumor localization. This promising ADC contrast has been explored *in vivo*, as recently summarized by Pickles *et al.* [1]. Nevertheless, none of the reports to date validated the suspected PCa region, either diagnosed by T2W, ADC contrast, or biopsy, with the "gold standard" histology. Herein, we propose a co-registration strategy to determine the *in vivo* ADC of histology identified PCa.

Material and methods

Patients Twelve radical prostatectomy patients (mean age 62 yrs, range 46 – 76 yrs) without any preoperative treatment were enrolled in this study.

MRI *In vivo* diffusion tensor imaging (DTI) measurement (resolution = 2×2×2.5 mm) and T2W imaging (resolution = 1×1×2.5 mm) were performed prior to scheduled prostatectomy surgery [2]. After surgery, prostatectomy specimens were fixed in formalin for more than 24 hours and step-sectioned at 4-mm intervals using a custom-made slicer. The regrouped 4-mm tissue blocks underwent ultra high resolution (0.5×0.5×0.5 mm) *ex vivo* DTI measurement [3].

Histology Individual 4-mm sections were carefully labeled to ensure correct identification of each section within the prostate. The sectioned slabs were then completely embedded in paraffin and sampled in 4-μm thick slices for hematoxylin and eosin (H & E) staining. Regions of PCa and BPH were identified and outlined in blue and red, respectively, by a urologic pathologist.

Image registration A two-dimensional (2D) thin plate spline (TPS) warping was performed using 10 – 20 control points (Fig 2, A and B) to transform histology to the coordinate of *ex vivo* ADC map (Fig. 1, T1). By using a rigid body 3D affine transformation (Fig. 1, T2), the *ex vivo* ADC maps were further manually co-registered with the *in vivo* T2W images through intra-glandular structure alignment. The *in vivo* ADC maps were also co-registered with the *in vivo* T2W images using a 3D affine transformation (Fig. 1, T3). In this manner, all the images were mutually aligned in the coordinate space of the standard *in vivo* T2W images.

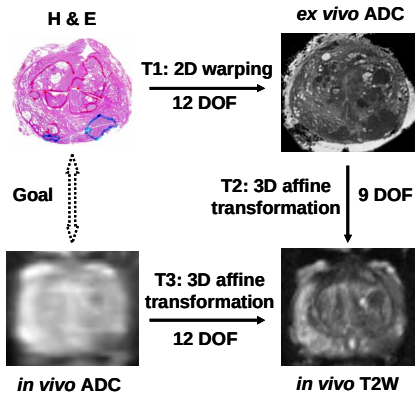

Figure 1. Overview of histology and *in vivo* ADC co-registration.

Results and Discussions

The ultra high resolution *ex vivo* diffusion anisotropy map (Fig. 2B), revealing exquisite intra-glandular structure, affords accurate placement of the control points in the corresponding histology slide (Fig. 2A). The *ex vivo* ADC map, exhibiting similar tissue contrast as the *in vivo* T2W images, provides a critical link to the *in vivo* ADC map. Excellent co-registration results were achieved despite some manual procedures involved (Fig. 3). The registration results may be further improved by utilizing mutual information based automatic procedures [4]. After image registration, cancerous (Fig. 2D) and normal (Fig. 2C) tissues in the PZ were mapped from the histology slides onto the *in vivo* and *ex vivo* ADC maps to determine the ADC values in each tissue category. The ADC values in PCa is consistently much lower than that in normal tissues (Fig. 4) in *in vivo* patients, *ex vivo* prostatectomy specimens, and an *in vivo* mouse model of PCa [5].

Reference [1] Pickles, *et al. J. Magn. Reson. Imaging* **23**, 130, 2006. [2] Xu, *et al. Proc. Intl. Soc. Magn. Reson. Med.* **13**, 2125, 2005. [3] Xu, *et al. Proc. Intl. Soc. Magn. Reson. Med.* **12**, 2508, 2004. [4] Meyer, *et al. Mol. Imaging* **13**, 16, 2006. [5] Song, *et al. Cancer Res.* **62**, 1555, 2002.

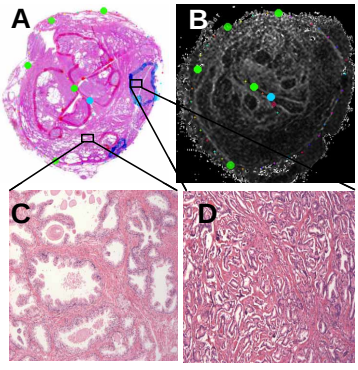

Figure 2. Representative control points that drive the 2D TPS warping in the T1 transformation are enlarged in both the H&E slide (A) and the *ex vivo* diffusion anisotropy map (B). Cancerous (marked blue in A) and non-cancerous PZ, identified by pathologist, are magnified to show the more cellular PCa (D) comparing to the normal ductal tissues (C).

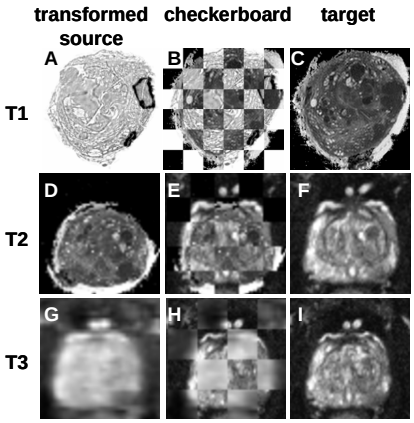

Figure 3. Registration results at three transformation stages (rows, T1 - T3). The transformed source images (left column) were overlaid onto the target images (right column) to highlight alignment results in checkerboards (center column). The transformation pairs are A) TPS warped H&E and C) *ex vivo* ADC; D) transformed *ex vivo* ADC and F) *in vivo* T2W; and G) transformed *in vivo* ADC and I) *in vivo* T2W.

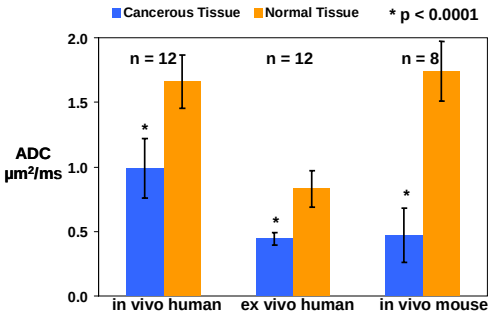

Figure 4. Decreased ADC values were observed in *in vivo* patients, *ex vivo* human prostatectomy specimens, and an *in vivo* mouse model of PCa. All results were determined by histopathology identified tissue categories. Error bars represent mean standard deviation. Statistical significance was accepted for $p < 0.0001$.

Exclusion of False Positive Identification of Prostate Cancer Using Diffusion Anisotropy

J. G. Xu[1], P. A. Humphrey[2], A. S. Kibel[3], V. R. Narra[4], S-K. Song[4]

[1]Chemistry, Washington University in St. Louis, St. Louis, Missouri, United States, [2]Pathology & Immunology, Washington University in St. Louis, St. Louis, Missouri, United States, [3]Surgery, Washington University in St. Louis, St. Louis, Missouri, United States, [4]Radiology, Washington University in St. Louis, St. Louis, Missouri, United States

Introduction

The normal prostate comprises a branching duct-acinar glandular system embedded in a dense fibromuscular stroma. The substantial decrease of mean water diffusivity due to disruption of the ductal structures by prostate cancer (PCa) provides unique contrast for tumor localization. However, it is difficult to distinguish PCa from benign prostatic hyperplasia (BPH) on the basis of changes in mean diffusivity alone because both processes affect this diffusion parameter. An alternative means of distinguishing PCa and BPH is through measures of diffusion anisotropy, which has not yet been systematically evaluated in this role. To examine the potential utility of diffusion anisotropy for PCa identification, the prostates from thirteen radical prostatectomy patients were examined by diffusion tensor imaging (DTI) *in vivo* before surgery, and *ex vivo* after surgery and formalin fixation. DTI findings were validated by co-registered histology.

Material and methods

MRI *In vivo* DTI was performed on a 1.5-tesla scanner using a phased-array body coil at 2 × 2 × 2.5 mm resolution. Diffusion sensitizing gradients were applied along six directions. Two diffusion sensitizing factors or *b* values = 0 and 500 s/mm^2 were used to calculate the apparent diffusion coefficient (ADC) and scaled relative anisotropy (sRA). Additionally, fat saturated T_2 weighted (T2W) images were acquired at 1 × 1 × 2.5 mm resolution. After surgery, prostatectomy specimens were fixed in formalin for more than 24 hours and step-sectioned at 4-mm intervals. The 4-mm sections were regrouped with a thin sheet of susceptibility matched spacer inserted between adjacent sections for MRI slice prescription. Ultra high resolution (0.125 mm^3 voxel size) *ex vivo* DTI, employing parameters reported previously [1], was performed on the regrouped slices.

Histology Individual 4-mm sections were carefully labeled to ensure correct identification of each section within the prostate. The sectioned slabs were then completely embedded in paraffin and sampled in 4 μm thick slices for hematoxylin and eosin (H & E) stains. Regions of PCa and BPH were identified and outlined in blue and red, respectively, by a urologic pathologist. The diffusion weighted (DW) images obtained *in vivo* were co-registered with the higher resolution *in vivo* T2W images, then with the even higher resolution *ex vivo* DW images, and finally with the optical microscopy images using algorithms based on 3D affine transformation and normalized mutual information.

Results and Discussions

The expanding nodules of BPH push and tighten the normal fibromuscular system around them, resulting in ordered fiber bundles with networked structure in the sRA map (Fig. 1 A). Diffusion anisotropy was higher in these ordered, compressed areas (0.34 ± 0.08, Figs. 1 B – D) compared to that of the acinar glandular tissues and PCa, for which sRA was 0.13 ± 0.05 *ex vivo* ($n = 13$, $p < 0.001$). A similar differential holds for *in vivo* diffusion anisotropy measures. sRA values were 0.13 ± 0.07 for fibromuscular tissue compared with 0.05 ± 0.02 for glandular tissue and PCa ($n = 13$, $p < 0.001$). The sRA for both types of tissues are smaller *in vivo* than *ex vivo* due to the lower image resolution and the resulting partial volume effects for the *in vivo* data. We found that diffusion anisotropy remains low both *in vivo* and *ex vivo* in the glandular tissues regardless of the presence of PCa, as also noted by Reinsberg *et al.* [2]. In light of our preliminary experimental observations and the expected tissue microstructure changes, we propose that high diffusion anisotropy can be used as an exclusion criterion for PCa diagnosis. As noted above, areas of BPH may exhibit PCa-like contrast on both the T2W images (black arrow, Fig. 2 A) and ADC maps (black arrow, Fig. 2 B), which could lead to a false positive diagnosis. In all three patients with BPH mimicking PCa, the presence of elevated diffusion anisotropy (black arrow, Fig 2 C) reliably prevents a false positive identification of PCa. The validity of this identification was confirmed by the corresponding histology (Fig. 2 D). In the representative case shown here, the area of reduced ADC (black arrow, Figs. 2 A – D) corresponds to a stromal BPH nodule (Figs. 2 E - F). Despite the much smaller diffusion anisotropy magnitude and differential *in vivo*, the presence of elevated anisotropy was sufficient to prevent misidentification of BPH as PCa.

Reference [1] Xu, *et al. Proc. Intl. Soc. Mag. Reson. Med.* **12**, 2508, 2004. [2] Reinsberg, *et al. Proc. Intl. Soc. Mag. Reson. Med.* **13**, 269, 2005.

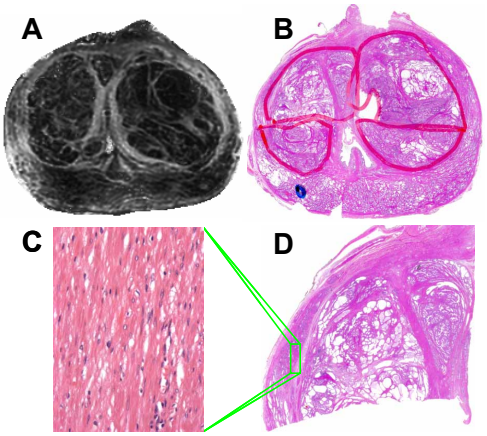

Figure 1. Corresponding *ex vivo* sRA map (A) and H & E stains (B) with PCa and BPH outlined in blue and red, respectively. The high diffusion anisotropy region in the top left quadrant of the histology slide (D) was further examined at 20 × magnification (C).

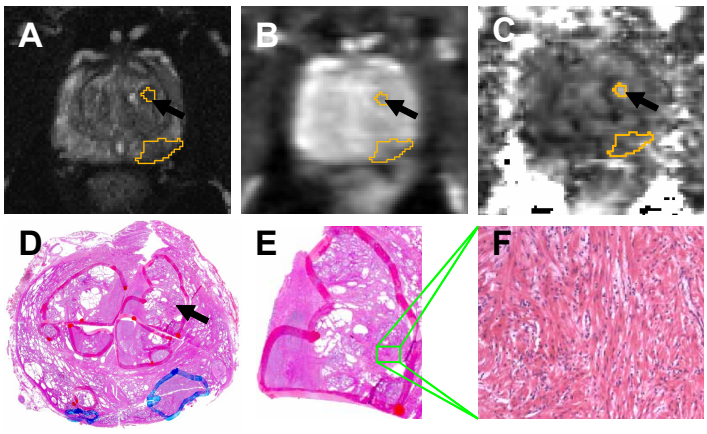

Figure 2. Corresponding *in vivo* T2W image (A), ADC map (B), sRA map (C), and H & E stains (D) with PCa and BPH outlined in blue and red, respectively. Using ADC contrast only, the suspected PCa regions were outlined in orange (B) and mapped onto the T2W image (A) and sRA map (C). The high diffusion anisotropy region (black arrow) was histologically verified as a BPH nodule (E), with its stromal structure revealed at 20 × magnification (F).